Impact of sub-pixel variations on ocean color remote sensing products

Article *in* Optics Express · September 2012

DOI: 10.1364/OE.20.020844 · Source: PubMed

4 authors, including:

Zhongping Lee
University of Massachusetts Boston
152 PUBLICATIONS **6,289** CITATIONS

SEE PROFILE

Robert Arnone
University of Southern Mississippi
277 PUBLICATIONS **6,118** CITATIONS

SEE PROFILE

Zhen Liu
Shandong University of Science and Technology
4 PUBLICATIONS **34** CITATIONS

SEE PROFILE

Impact of sub-pixel variations on ocean color remote sensing products

Zhongping Lee,[1,*] Chuanmin Hu,[2] Robert Arnone,[3] and Zhen Liu[1]

[1] *Department of Environmental, Earth and Ocean Sciences, University of Massachusetts, Boston, Massachusetts 02125, USA*

[2] *College of Marine Science, University of South Florida, St. Petersburg, Florida 33701, USA*

[3] *Naval Research Laboratory, Stennis Space Center, Mississippi 39529, USA*

**Zhongping.lee@umb.edu*

Abstract: Passive remote sensing of the Earth system has used spatial resolutions ranging from meters to kilometers. It is thus necessary to understand how data products with different spatial resolutions can be compared with each other, and how sub-pixel variations may affect data comparison. This is particularly important for ocean color remote sensing where the measured signal (water-leaving radiance or remote sensing reflectance) is a non-linear function of sub-surface constituents. As a result, products at low resolution are not necessarily arithmetic or geometric means of those at higher resolution. Here, we developed analytical expressions to link ocean color properties derived from high- and low-resolution data, and the proof-of-concept is further demonstrated with both simple examples and measurements of MERIS full-resolution (FR) and reduced resolution (RR). These results suggest that current global chlorophyll concentration is likely underestimated due to the coarse spatial resolutions. Application of the expressions will facilitate cross-sensor comparisons and may also reduce uncertainties.

OCIS codes: 010.4450 Oceanic optics; 010.0280 Remote sensing and sensors.

References and links

1. L. B. Eisner and T. J. Cowles, "Spatial variations in phytoplankton pigment ratios, optical properties, and environmental gradients in Oregon coast surface waters," J. Geophys. Res. **110**(C10), C10S14 (2005), doi:10.1029/2004JC002614.
2. C. Hu, B. Nababan, D. C. Biggs, and F. E. Muller-Karger, " Variability of bio-optical properties at sampling stations and implications for remote sensing: a case study in the north-east Gulf of Mexico," Int. J. Remote Sens. **25**(11), 2111–2120 (2004).
3. C. B. Schaaf, F. Gao, A. Strahler, W. Lucht, X. Li, T. Tsang, N. C. Strugnell, X. Zhang, Y. Jin, J. P. Muller, P. Lewis, M. Barnsley, P. Hobson, M. Disney, G. Roberts, M. Dunderdale, C. Doll, R. P. d'Entremont, B. Hu, S. Liang, J. L. Privette, and D. Roy, "First Operational BRDF, Albedo and Nadir reflectance products from MODIS," Remote Sens. Environ. **83**(1-2), 135–148 (2002).
4. H. R. Gordon and D. K. Clark, "Remote sensing optical properties of a stratified ocean: an improved interpretation," Appl. Opt. **19**(20), 3428–3430 (1980).
5. S. Sathyendranath and T. Platt, "Remote sensing of ocean chlorophyll: consequence of nonuniform pigment profile," Appl. Opt. **28**(3), 490–495 (1989).
6. J. R. V. Zaneveld, A. H. Barnard, and E. Boss, "Theoretical derivation of the depth average of remotely sensed optical parameters," Opt. Express **13**(22), 9052–9061 (2005).
7. H. R. Gordon and A. Morel, *Remote assessment of ocean color for interpretation of satellite visible imagery: A review* (New York: Springer-Verlag 1983) p. 44.
8. IOCCG, *Remote Sensing of Inherent Optical Properties: Fundamentals, Tests of Algorithms, and Applications, in Reports of the International Ocean-Colour Coordinating Group*, No. 5, Z.-P. Lee, ed. (IOCCG: Dartmouth, Canada. 2006) p. 126.
9. H. R. Gordon, O. B. Brown, R. H. Evans, J. W. Brown, R. C. Smith, K. S. Baker, and D. K. Clark, "A semianalytic radiance model of ocean color," J. Geophys. Res. **93**(D9), 10909–10924 (1988).
10. Z. P. Lee, K. Du, K. J. Voss, G. Zibordi, B. Lubac, R. Arnone, and A. Weidemann, "An inherent-optical-property-centered approach to correct the angular effects in water-leaving radiance," Appl. Opt. **50**(19), 3155–3167 (2011).

#172216 - $15.00 USD Received 10 Jul 2012; revised 23 Aug 2012; accepted 24 Aug 2012; published 28 Aug 2012

11. A. Morel and B. Gentili, "Diffuse reflectance of oceanic waters (2): Bi-directional aspects," Appl. Opt. **32**(33), 6864–6879 (1993).
12. C. D. Mobley, *Light and Water: radiative transfer in natural waters* (New York: Academic Press 1994).
13. C. Hu, Z. Chen, T. D. Clayton, P. Swarzenski, J. C. Brock, and F. E. Muller-Karge, "Assessment of estuarine water-quality indicators using MODIS medium-resolution bands: Initial results from Tampa Bay Florida," Remote Sens. Environ. **93**(3), 423–441 (2004).
14. M. Darecki and D. Stramski, "An evaluation of MODIS and SeaWiFS bio-optical algorithms in the Baltic Sea," Remote Sens. Environ. **89**(3), 326–350 (2004).
15. F. Mélin, G. Zibordi, and J.-F. Berthon, "Assessment of satellite ocean color products at a coastal site," Remote Sens. Environ. **110**(2), 192–215 (2007).
16. S. Shang, Z. Lee, and G. Wei, " Characterization of MODIS-derived euphotic zone depth: results for the China Sea," Remote Sens. Environ. **115**(1), 180–186 (2011).
17. R. M. Pope and E. S. Fry, "Absorption spectrum (380-700 nm) of pure water. II. Integrating cavity measurements," Appl. Opt. **36**(33), 8710–8723 (1997).
18. H. R. Gordon, M. R. Lewis, S. D. McLean, M. S. Twardowski, S. A. Freeman, K. J. Voss, and G. C. Boynton, "Spectra of particulate backscattering in natural waters," Opt. Express **17**(18), 16192–16208 (2009).
19. Z. P. Lee, K. L. Carder, and K. P. Du, "Effects of molecular and particle scatterings on the model parameter for remote-sensing reflectance," Appl. Opt. **43**(25), 4957–4964 (2004).
20. Z. P. Lee, K. L. Carder, C. D. Mobley, R. G. Steward, and J. S. Patch, "Hyperspectral remote sensing for shallow waters: 2. Deriving bottom depths and water properties by optimization," Appl. Opt. **38**(18), 3831–3843 (1999).
21. S. Sathyendranath and T. Platt, "Analytic model of ocean color," Appl. Opt. **36**(12), 2620–2629 (1997).
22. Z. Lee, V. P. Lance, S. Shang, R. Vaillancourt, S. Freeman, B. Lubac, B. R. Hargreaves, C. Del Castillo, R. Miller, M. Twardowski, and G. Wei, "An assessment of optical properties and primary production derived from remote sensing in the Southern Ocean (SO GasEx)," J. Geophys. Res. **116**, C00F03 (2011), doi:10.1029/2010JC006747.
23. C. Hu, Z. Lee, and B. Franz, "Chlorophyll a algorithms for oligotrophic oceans: A novel approach based on three-band reflectance difference," J. Geophys. Res. **117**(C1), C01011 (2012), doi:10.1029/2011JC007395.
24. J. E. O'Reilly, "SeaWiFS Postlaunch Calibration and Validation Analyses," Part 3, in SeaWiFS Postlaunch Technical Report Series, S.B. Hooker and E.R. Firestone, Editors. 2000, NASA Goddard Space Flight Center: Greenbelt, MD. p. 58.
25. F. C. Polcyn, W. L. Brown, and I. J. Sattinger, "The measurement of water depth by remote-sensing techniques," University of Michigan: Ann Arbor (1970).
26. D. R. Lyzenga, "Passive remote-sensing techniques for mapping water depth and bottom features," Appl. Opt. **17**(3), 379–383 (1978).
27. C. D. Mobley, L. K. Sundman, C. O. Davis, J. H. Bowles, T. V. Downes, R. A. Leathers, M. J. Montes, W. P. Bissett, D. D. R. Kohler, R. P. Reid, E. M. Louchard, and A. Gleason, "Interpretation of hyperspectral remote-sensing imagery by spectrum matching and look-up tables," Appl. Opt. **44**(17), 3576–3592 (2005).
28. V. E. Brando, J. M. Anstee, M. Wettle, A. G. Dekker, S. R. Phinn, and C. Roelfsema, "A physics based retrieval and quality assessment of bathymetry from suboptimal hyperspectral data," Remote Sens. Environ. **113**(4), 755–770 (2009).
29. S. Maritorena, A. Morel, and B. Gentili, "Diffuse reflectance of oceanic shallow waters: influence of water depth and bottom albedo," Limnol. Oceanogr. **39**(7), 1689–1703 (1994).
30. Z. P. Lee, K. L. Carder, R. F. Chen, and T. G. Peacock, " Properties of the water column and bottom derived from Airborne Visible Infrared Imaging Spectrometer (AVIRIS) data," J. Geophys. Res. **106**, 11639–11652 (2001).
31. Z. P. Lee, B. Casey, R. A. Arnone, A. D. Weidemann, A. R. Parsons, M. Montes, B. C. Gao, W. A. Goode, C. Davis, and J. Dye, "Water and bottom properties of a coastal environment derived from Hyperion data measured from the EO-1 spacecraft platform," J. Appl. Remote Sens. **1**(1), 011502 (2007).
32. Z. P. Lee, K. L. Carder, and R. A. Arnone, "Deriving inherent optical properties from water color: a multiband quasi-analytical algorithm for optically deep waters," Appl. Opt. **41**(27), 5755–5772 (2002).
33. P. Bontempi and J. Yoder, "Spatial variability in SeaWiFS imagery of the South Atlantic bight as evidenced by gradients (fronts) in chlorophyll a and water-leaving radiance," Deep Sea Res., Part II **51**(10–11), 1019–1032 (2004).
34. C. O. Davis, M. Kavanaugh, R. Letelier, W. P. Bissett, and D. Kohler, "Spatial and Spectral Resolution Considerations for Imaging Coastal Waters," in SPIE Coastal Ocean Remote Sensing. 2007. San Diego, CA.

1. Introduction

Remote sensing plays an indispensable role for the acquisition of geophysical information of large areas. These missions employ various platforms including aircraft and satellites, with sensors measuring the Earth's surface at resolutions ranging from sub-meters to kilometers. For instance, an image pixel from the WorldView 2 satellite measurement has a size of ~1.5 x 1.5 meter (high spatial resolution), while a pixel from Hyperion or Landsat measurement is ~30 x 30 m, and a pixel from the Moderate-resolution Imaging Spectroradiometer (MODIS)

#172216 - $15.00 USD Received 10 Jul 2012; revised 23 Aug 2012; accepted 24 Aug 2012; published 28 Aug 2012

or the Sea-viewing Wide Field-of-view Sensor (SeaWiFS) measurement is ~1000 x 1000 m (medium spatial resolution). Thus, one MODIS pixel encompasses ~33 x 33 Hyperion or Landsat pixels and ~660 x 660 WorldView 2 pixels. The high-resolution measurements provide detailed information for a targeted area, while the low-resolution measurements provide synoptic information over larger areas. On the other hand, this spatial mismatch produces difficulties in comparing products measured with different spatial resolutions when the target is inhomogeneous [1, 2]. For a spatially homogeneous environment, it is easy to visualize that the product of a unit area (e.g., absorption coefficient, concentration of chlorophyll) of a low-resolution pixel is equivalent to the product of any pixel of high-resolution pixels encompassed by the low-resolution pixel. For a spatially inhomogeneous environment, the situation becomes complex. For information mainly generated from a 2-dimensional (horizontal) domain such as surface temperature or Earth surface albedo [3], normally an arithmetic mean of the high-resolution measurements can represent the low-resolution measurements. For ocean color remote sensing, however, because of its 3-dimensional (horizontal and vertical) characteristics, it is not known if this arithmetic mean is still representative. For instance, for vertically stratified waters, the remotely observed property is not a simple arithmetic mean of its vertical profile, but a weighted mean with the weight decreased exponentially with increasing depth [4–6]. The same argument also applies to horizontally inhomogeneous waters (see Fig. 1 for instance): although the water-leaving radiance from a low-resolution pixel is an arithmetic mean of those from the corresponding higher-resolution pixels, the non-linear nature of the dependence between water-leaving radiance and sub-surface constituents makes it non-straightforward to extend the "averaging" concept to the retrieved data products. This raises the question of how best to compare products measured with different spatial resolutions? The same question is also raised in planning field measurements for the validation of remote sensing products [2], where discrete point measurements are used to compare with the synoptic data from the remote sensing estimates.

Based on established radiative transfer models for ocean color remote sensing, this short letter addresses these questions for water and bottom properties, with the ultimate objective of providing an analytical solution for comparing products at different resolutions. In addition, it tries to provide an easy understanding of low-resolution product for spatially inhomogeneous environments. Because of the particular importance of sub-pixel variations in optically shallow waters where the bottom contributes to a significant amount of satellite signal, we address these questions for two distinctive environments: optically deep and optically shallow waters.

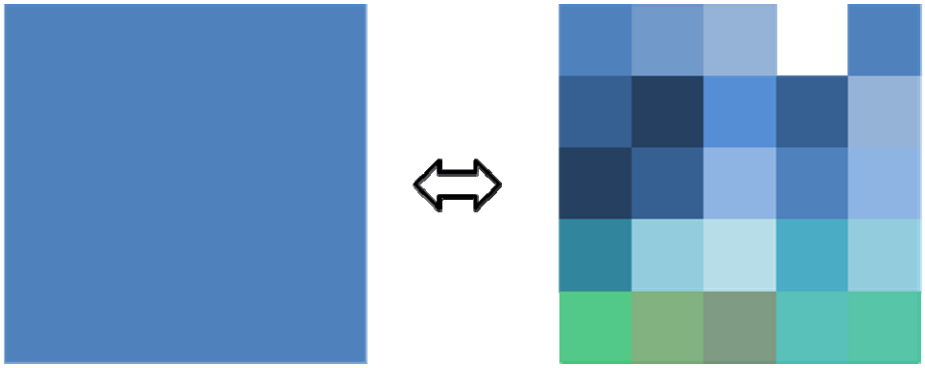

Fig. 1. (left) A pixel observed by a low-resolution sensor; (right) Pixels observed by a high-resolution sensor, corresponding to the low-resolution pixel.

#172216 - $15.00 USD Received 10 Jul 2012; revised 23 Aug 2012; accepted 24 Aug 2012; published 28 Aug 2012

Optically Deep waters

After radiometric calibration and atmospheric correction, the fundamental property of ocean color remote sensing is the remote sensing reflectance (*Rrs*, sr^{-1}), which is used for the derivation of subsurface properties [7, 8]. *Rrs* is defined as the ratio of water-leaving radiance (L_w, mW cm^{-2} μm^{-1} sr^{-1}) to downwelling irradiance just above the surface (E_d, mW cm^{-2} μm^{-1}). For optically deep waters, *Rrs* can be expressed as [9] (a more detailed review is provided in Lee et al [10])

$$Rrs = G\left(g_0 + g_1 \frac{b_b}{a+b_b}\right)\frac{b_b}{a+b_b}. \quad (1)$$

Here G is a dimensionless parameter representing the cross-surface effect [11, 12], $g_{0,1}$ (sr^{-1}) are model coefficients and they are constants for a given water body and sensor-sun geometry; a (m^{-1}) and b_b (m^{-1}) are the absorption and backscattering coefficients, respectively. a is composed of the contribution of pure seawater, phytoplankton pigments, colored dissolved organic matter (CDOM), and detrital particles; while b_b is composed of contribution of pure seawater and suspended particulates [12].

For *Rrs* of a low-resolution pixel (Rrs^{Lo}), Eq. (1) becomes

$$Rrs^{Lo} = G\left(g_0 + g_1 \frac{b_b{}^{Lo}}{a^{Lo}+b_b{}^{Lo}}\right)\frac{b_b{}^{Lo}}{a^{Lo}+b_b{}^{Lo}}, \quad (2)$$

where a^{Lo} and $b_b{}^{Lo}$ are the "effective" absorption and backscattering coefficients of the pixel. Here the term "effective" refers to the perceived optical properties that make up Rrs^{Lo}.

Now consider n high-resolution pixels that make up the low-resolution pixel. For each Rrs^{Lo}, because the downwelling irradiance on each high-resolution pixel is virtually the same, Rrs^{Lo} is the arithmetic mean of Rrs^{Hi} from the n high-resolution pixels,

$$Rrs^{Lo} = \overline{Rrs^{Hi}(i)}. \quad (3)$$

Here i represents the high-resolution pixel index. Because *Rrs* is not proportional to a (rather to $1/a$ in general), Eqs. (1-3) indicate the following is generally true:

$$a^{Lo} \neq \overline{a^{Hi}(i)}. \quad (4)$$

It is then desired and important to know what a^{Lo} means for spatially inhomogeneous waters, especially when satellite products are compared with field data [13–16] or when satellite products with different spatial resolutions are compared with each other.

For easier derivation and explanation, we use the following simplified model [11] to describe the relationship between *Rrs* and a and b_b,

$$Rrs \approx g' \frac{b_b}{a}, \quad (5)$$

Here parameter g' includes both cross-surface effects as well as the modeling coefficients between *Rrs* and inherent optical properties (IOPs; a and b_b, in particular). Then, the arithmetic mean of $Rrs^{Hi}(i)$ becomes the arithmetic mean of $\frac{b_b(i)}{a(i)}$; and from Eq. (3), there is

$$g' \frac{b_b{}^{Lo}}{a^{Lo}} \approx \overline{g' \frac{b_b{}^{Hi}(i)}{a^{Hi}(i)}}. \quad (6)$$

#172216 - $15.00 USD Received 10 Jul 2012; revised 23 Aug 2012; accepted 24 Aug 2012; published 28 Aug 2012

Because g' is relatively stable [9, 11] and considered not to vary significantly within the high-resolution pixels, the above relationship is reduced to

$$\frac{b_b^{Lo}}{a^{Lo}} \approx \frac{1}{n}\sum_{i=1}^{n}\frac{b_b^{Hi}(i)}{a^{Hi}(i)}. \tag{7}$$

Simple algebraic manipulations lead to

$$a^{Lo} \approx \frac{n\, b_b^{Lo}\prod_{i=1}^{n} a^{Hi}(i)}{\sum_{i=1}^{n}\left(b_b^{Hi}(i)\prod_{j=1,j\neq i}^{n-1} a^{Hi}(j)\right)}. \tag{8}$$

Here $\prod_{j=1,j\neq i}^{n-1} a^{Hi}(j)$ represents multiplication of all a^{Hi} except $a^{Hi}(i)$ when $b_b^{Hi}(i)$ is used.

Further, because Rrs is generally linearly proportional to particle backscattering coefficient (b_b, see Eq. (5)) and because absorption at longer wavelengths (except absorption peaks of various phytoplankton pigments) is nearly stable [12, 17], b_b^{Lo} in the longer wavelengths can then be derived following Eq. (6) as

$$b_b^{Lo} \approx \overline{b_b^{Hi}(i)}. \tag{9}$$

This formulation is expended to shorter wavelengths based on the fact that the spectral variation of b_b follows a simple power-law function [7, 18]. Thus, Eqs. (8) and (9) show how the effective b_b^{Lo} and a^{Lo} can be derived from their high-resolution measurements. Equation (8) further indicates that, because Rrs^{Lo} represents the arithmetic mean of Rrs^{Hi} (see Eq. (3)), if the high-resolution pixels are not homogeneous (e.g., in frontal zones, coastal waters, etc.), a^{Lo} derived from Rrs^{Lo} is the backscattering-weighted mean of a^{Hi} instead of an arithmetic mean of a^{Hi}.

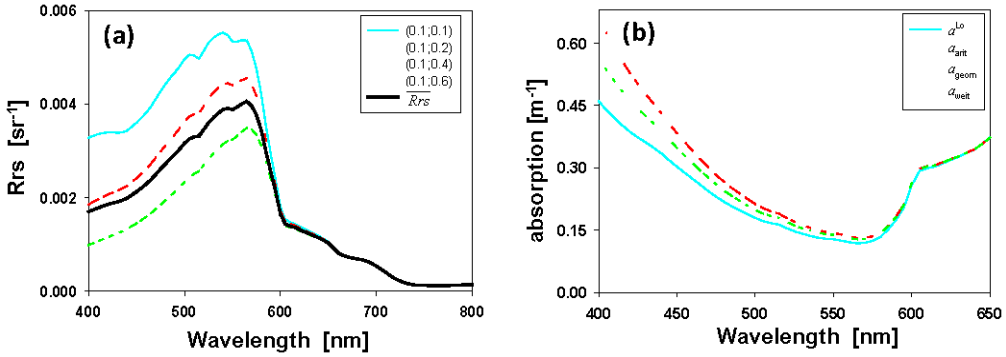

Fig. 2. (a) *Rrs* of 4 high-resolution pixels and their average. First value and second value in the parenthesis are the absorption coefficient of phytoplankton and CDOM at 440 nm, respectively. (b) Absorption spectrum derived from the average *Rrs* (blue line), as compared with the average absorption spectra using various schemes, including arithmetic mean, geometric mean, and backscattering-weighted mean (Eq. (8)).

Table 1. Symbol and definition of spatially averaged properties.

Symbol	Definition
P^{Lo}	Property (P) perceived by a low-resolution sensor
P_{arit}	Arithmetic mean of high-resolution observation of property P
P_{geom}	Geometric mean of high-resolution observation of property P
P_{weig}	Weighted mean of high-resolution observation of property P

Figure 2 shows an example to demonstrate this concept. *Rrs* spectra of 4 high-resolution pixels were simulated with the Lee et al [19] IOP-*Rrs* model. In this simple illustration, the 4

#172216 - $15.00 USD Received 10 Jul 2012; revised 23 Aug 2012; accepted 24 Aug 2012; published 28 Aug 2012

pixels had the same phytoplankton absorption and particle backscattering coefficients while the absorption coefficient of colored dissolved organic matter (CDOM) was varied from 0.1 to 0.6 m^{-1}. The *Rrs* spectrum perceived from the low-resolution pixel encompassing all 4 high-resolution pixels was calculated as an arithmetic mean (Eq. (3)), as shown in Fig. 2(a) (black line). From a spectral optimization inversion algorithm [20], *a* was derived from Rrs^{Lo} and shown in Fig. 2(b) as a^{Lo} (see Table 1 for definition of symbols). The arithmetic (and geometric) mean of absorption from the 4 high-resolution pixels showed much higher values (about 29% and 22% at 410 nm and 440 nm, respectively) in the blue-green wavelengths than a^{Lo} (see Fig. 2(b)). In contrast, the weighted mean, a_{weit}, calculated with Eqs. (8) and (9) from Rrs^{Lo}, closely (average absolute percentage difference is ~1.1%) follows a^{Lo}.

These results clearly showed that the absorption coefficients in the shorter wavelengths perceived by a low-resolution pixel is much lower than the arithmetic mean of that from the high-resolution pixels, but it could be well represented by the backscattering-weighted mean. This result further suggests that the chlorophyll concentrations derived from low-resolution measurements are likely underestimated compared to that measured by high-resolution measurements, as the empirically derived chlorophyll concentration closely follows the total absorption coefficient [21–23]. Specifically for the examples shown in Fig. 2, using the same OC4 algorithm [24], the arithmetic mean chlorophyll concentration of the 4 high-resolution pixels are 5.4 mg/m^3, but it is 4.7 mg/m^3 from Rrs^{Lo}, which is reduced by ~13%. Note that empirical band-ratio algorithms do not distinguish the impacts of phytoplankton and CDOM, so the variation of CDOM is perceived as variation of phytoplankton (Chl-a).

Optically shallow bottom

It has long been demonstrated that the depth of optically shallow bottom could be retrieved from spectral measurements of water color [25–28]. On the other hand, bottom depth (*H*, m) in shallow waters may change substantially in a small region, creating a similar problem to the above when comparing bottom depths derived from remote sensing measurements at different spatial resolutions. To address this problem, analytical expressions to relate low-resolution and high-resolution bottom depth products, such as Eq. (8) for optically deep waters, are investigated here.

Rrs of optically shallow waters can be expressed as [20, 29]

$$\begin{aligned} Rrs &= G\left(r_{rs}^{C} + r_{rs}^{B}\right) \\ &= G\left[\, r_{rs}^{dp}\left(1 - e^{-D_c(a+b_b)H}\right) + \frac{\rho}{\pi} e^{-D_B(a+b_b)H} \,\right]. \end{aligned} \tag{10}$$

Here r_{rs}^{C} and r_{rs}^{B} are the sub-surface remote-sensing reflectance from the water column and the shallow bottom, respectively; ρ represents the bottom reflectance (albedo), while $D_{c,B}$ is the path-elongation factor for the water column and bottom returned photons, respectively. r_{rs}^{dp} is the sub-surface remote-sensing reflectance of the same water column with an infinite depth. Clearly, compared to optically deep waters, the cross-pixel variations of inhomogeneous systems make it even harder to interpret low-resolution retrievals.

To focus on the bottom depth retrievals, water properties (i.e., r_{rs}^{C}) are assumed homogenous across multiple high-resolution pixels (but within a low-resolution pixel) due to current and tidal mixing [30, 31]. Then, the following equations can be derived from Eq. (3) and Eq. (9):

$$\rho^{Lo} e^{-D_B(a+b_b)H^{Lo}} \approx \overline{\rho^{Hi}(i) e^{-D_B(a+b_b)H^{Hi}(i)}}. \tag{11}$$

and,

#172216 - $15.00 USD Received 10 Jul 2012; revised 23 Aug 2012; accepted 24 Aug 2012; published 28 Aug 2012

$$H^{Lo} \approx \frac{-1}{D_B(a+b_b)} \ln\left\{\frac{1}{\rho^{Lo}} \overline{\rho^{Hi}(i) e^{-D_B(a+b_b)H^{Hi}(i)}}\right\}. \quad (12)$$

The equations suggest that bottom depth derived from the low-resolution pixel (H^{Lo}) is not a simple average of bottom depths derived from the corresponding high-resolution pixels, and detailed information on both water column properties (a and b_b) and high-resolution bottom properties (depth and albedo) is required to explain the low-resolution H^{Lo}.

To help visualize this non-linear impact, consider that e^{-x} is proportional to $1/x$ for x in any narrow range, Eq. (11) can then be simplified as

$$\frac{\rho^{Lo}}{H^{Lo}} \approx \overline{\frac{\rho^{Hi}(i)}{H^{Hi}(i)}}. \quad (13)$$

Therefore,

$$H^{Lo} \approx \frac{n\ \rho^{Lo} \prod_{i=1}^{n} H^{Hi}(i)}{\sum_{i=1}^{n}\left(\rho^{Hi}(i) \prod_{j=1, j\neq i}^{n-1} H^{Hi}(j)\right)}. \quad (14)$$

Equation (14) shows that in order to interpret H^{Lo}, information of the low-resolution perceived bottom albedo (ρ^{Lo}) and the high-resolution bottom properties is required. In addition, unlike the case of backscattering coefficient of deep waters, ρ^{Lo} in general is not an arithmetic mean of $\rho^{Hi}(i)$ because the contribution of substrate from the multiple high-resolution pixels to a low-resolution pixel depends on both bottom albedo and depth. For a special case when the bottom albedo is uniform, Eq. (14) reduces to

$$H^{Lo} \approx \frac{n}{\sum_{i=1}^{n} \frac{1}{H^{Hi}(i)}}. \quad (15)$$

Similar to the deep-water example in Fig. 2, an example is shown in Fig. 3 to illustrate the non-linear effect of bottom depth on high- and low-resolution pixels. The example used homogenous water properties and bottom albedo but varying bottom depths (2 – 10 m) across 4 high-resolution pixels, and simulated their effect on the perceived bottom depth from a low-resolution pixel encompassing all 4 high-resolution pixels. The 4 high-resolution *Rrs* spectra (see Fig. 3(a)) were generated from a shallow-water model (see Eq. (10)), and the arithmetic mean of these *Rrs*, as measured from a low-resolution pixel, were fed back to the simulation model with H^{Lo} derived via spectral optimization [20]. The perceived H^{Lo} from Rrs^{Lo} is again much lower (~30% and 17%, respectively) than the arithmetic and geometric means of the four bottom depths, but agrees very well (within ~1% for this example) with that predicted by Eq. (15). This is consistent with radiative transfer as shallower bottom (assuming all other properties remain the same) results in greater radiance at sea surface and then contributes more to the total measured signal.

#172216 - $15.00 USD Received 10 Jul 2012; revised 23 Aug 2012; accepted 24 Aug 2012; published 28 Aug 2012

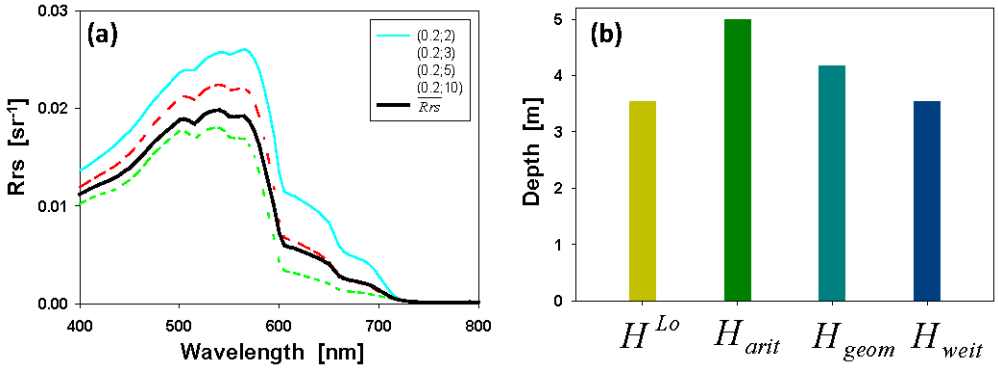

Fig. 3. (a) *Rrs* of 4 high-resolution pixels with varying bottom depth, and their arithmetic mean. Bottom reflectance (albedo) and water column properties are assumed the same. (b) Bottom depth derived from the average *Rrs*, H^{Lo}, as compared with the average bottom depth using various schemes.

Tests on MERIS measurements

The analyses and figures above demonstrate that water column and bottom depth properties derived from low-resolution data are lower than their arithmetic or geometric means derived from high-resolution data, and the former can be better described using a combination of high-resolution data and analytical equations similar to Eqs. (8), (14) and (15). To further prove this concept, satellite measurements from the Medium Resolution Imaging Spectrometer (MERIS) were used. MERIS measures the oceans at a nominal resolution of 300-m (full resolution or FR), while aggregated MERIS data have 1.2-km resolution (reduced resolution or RR), with 1 RR pixel corresponding to 16 FR pixels.

MERIS Level-2 data over the southern Ocean east of Argentina on 26 December 2011 were obtained from the U.S. NASA Goddard Flight Space Center (GSFC). The data contained spectral *Rrs* derived from the most recent updates in sensor calibration and processing algorithms embedded in the software package SeaDAS6.4. The FR *Rrs* (Rrs^{FR}) data for a meso-scale eddy were used with the quasi-analytical algorithm [32] to derive total absorption and backscattering coefficients at 440 nm, $a^{\mathrm{FR}}(440)$ (m^{-1}) and $B^{\mathrm{FR}}(440)$ (m^{-1}), respectively, at 300-m resolution. Then, $a^{\mathrm{FR}}(440)$ was aggregated to 1.2-km resolution to obtain arithmetic mean ($a_{arit}^{RR}(440)$), geometric mean ($a_{geom}^{RR}(440)$), and backscattering-weighted mean ($a_{weit}^{RR}(440)$) following Eq. (8). Further, $a^{\mathrm{RR}}(440)$ was derived from RR *Rrs* (Rrs^{RR}) data using the same algorithm and compared with the various means of $a^{\mathrm{FR}}(440)$ data.

#172216 - $15.00 USD Received 10 Jul 2012; revised 23 Aug 2012; accepted 24 Aug 2012; published 28 Aug 2012

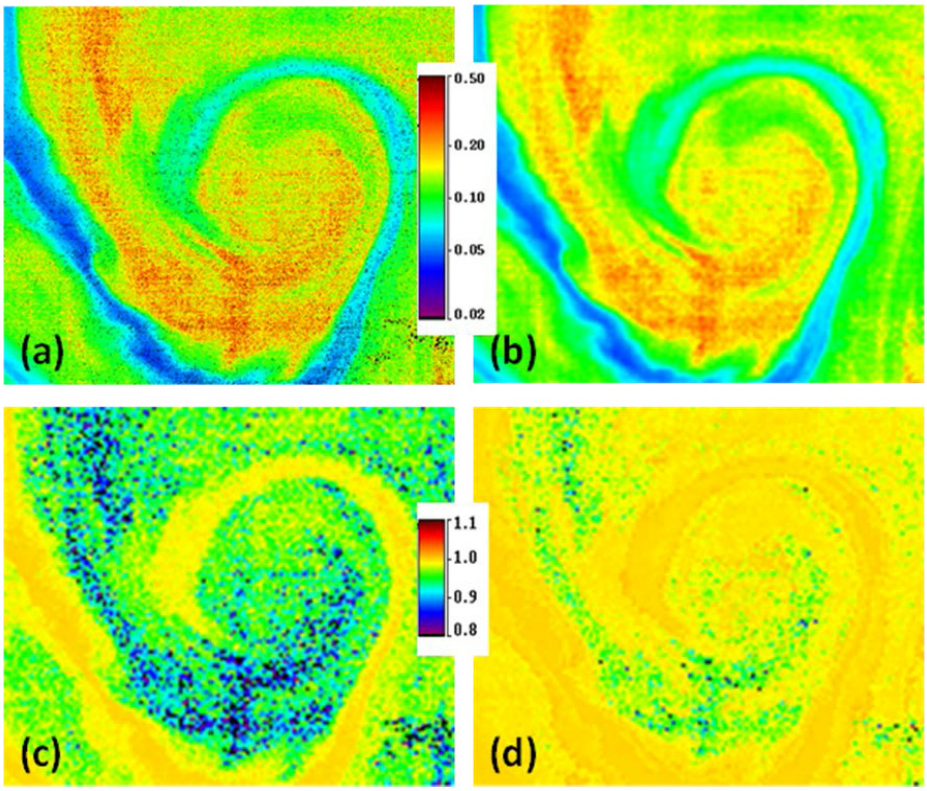

Fig. 4. MERIS measurements over the southern Ocean east of Argentina on 12/26/2011, 13:22 GMT, covering an area of about 163 x 134 km^2. (a) $a^{FR}(440)$ (m^{-1}) derived from the full-resolution (FR, 300 m) *Rrs* data using the QAA algorithm; (b) $a^{RR}(440)$ derived from the reduced-resolution (RR, 1.2 km) *Rrs* data using the same algorithm. 1 pixel in the RR image corresponds to 16 pixels in the FR image; (c) Ratio of $a^{RR}(440)$ over arithmetic mean of $a^{FR}(440)$; (d) Ratio of $a^{RR}(440)$ over backscattering-weighted mean of $a^{FR}(440)$ (Eq. (8)). Note that many pixels in (c) show ratios significantly lower than 1.0, as predicted in Fig. 2(b). Black points in (c) and (d) indicate clouds. The histograms of the ratios are shown below.

Figures 4(a) and 4(b) show $a^{FR}(440)$ and $a^{RR}(440)$, respectively; while the ratios of $a^{RR}(440)$ to $a_{arit}^{RR}(440)$ and $a_{weit}^{RR}(440)$, respectively, are calculated and shown in Figs. 4(c) and 4(d). Ratio of $a^{RR}(440)$ to $a_{geom}^{RR}(440)$ is also calculated but not shown (except its histogram, see Fig. 5). Compared with $a_{arit}^{RR}(440)$, $a^{RR}(440)$ is biased low for the patchy eddy (see Fig. 4(c)) where the ratio is often < 0.9. This trend is consistent with the simulation results in Fig. 2(b), although there are 16 FR pixels corresponding to 1 RR pixel here. In contrast, $a_{weit}^{RR}(440)$ agrees much better (see Fig. 5) with $a^{RR}(440)$, also consistent with the simulation results in Fig. 2(b). These contrasting results are further demonstrated in Fig. 5 where the histogram distributions of the $a(440)$ ratios clearly show the improvement in the backscattering-weighted mean when using high-resolution products to compare with low-resolution products.

#172216 - $15.00 USD Received 10 Jul 2012; revised 23 Aug 2012; accepted 24 Aug 2012; published 28 Aug 2012

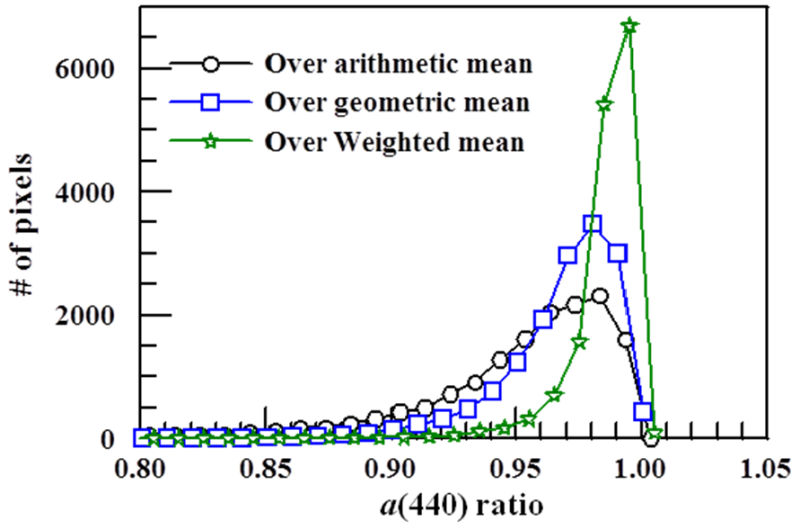

Fig. 5. Histograms of ratios between $a^{RR}(440)$ derived from MERIS RR data (1.2 km) and various averages of $a^{FR}(440)$ derived from MERIS FR (300 m) data. For any 1.2-km pixel, the average values over the corresponding sixteen 300-m pixels were calculated as arithmetic mean, geometric mean, and backscattering-weighted mean (Eq. (8)). The three ratios are 0.95 ± 0.54 (mean ± standard deviation), 0.97 ± 0.28, and 0.99 ± 0.14, respectively, while they are all skewed towards values < 1.0.

Implications for satellite remote sensing

The simulations and MERIS examples clearly show that when the water is patchy, low-resolution products are likely underestimated when compared to the "truth" (i.e., arithmetic mean of products from high-resolution measurements). This is simply because that the result of arithmetic mean favors higher values, and higher remote-sensing reflectance in the blue-green domain (the spectral window for sensing subsurface constituents or bottom depth) is likely associated with lower absorption or shallower bottom depth, although the actual situation will depend on the detailed spatial distribution of water and/or bottom properties. There are many cases where ocean waters are patchy [33, 34], for example in eddies, fronts, river plumes, or coastal blooms. Then, when high-resolution measurements are not available and there is substantial spatial variability, one can infer that the low-resolution products are possibly biased low. The same argument can also be applied for the global biomass standing stocks and for validation of satellite data using discrete field data. However, it is yet to be investigated to what degree the global biomass is underestimated due to a combination of ocean patchiness and low-spatial resolution measurement.

Conclusions

Analytical expressions are developed to provide an explicit interpretation of low resolution measurements and an easy way to remove uncertainties when comparing high-resolution and low-resolution data. It is found that the low-resolution product can be well represented using weighted means of high-resolution data. The concept has been demonstrated through simulations and satellite data analysis. These relationships provide insights into the spatial meaning of remote sensing products, especially for spatially inhomogeneous environments. Application of these relationships can reduce uncertainties when comparing measurements from platforms with different spatial resolutions. For spatially inhomogeneous environments, because remote-sensing reflectance (or water-leaving radiance) is a non-linear function of the water column constituents and bathymetry, products (e.g., chlorophyll-a concentration, CDOM absorption) derived from low-resolution measurements are likely biased low

#172216 - $15.00 USD Received 10 Jul 2012; revised 23 Aug 2012; accepted 24 Aug 2012; published 28 Aug 2012

compared to their arithmetic means from the corresponding high-resolution measurements. Thus, to overcome the uncertainty resulted in low- or medium-resolution measurements by ocean color sensors (e.g., SeaWiFS, MODIS), it is necessary to have concurrent high-resolution measurements (e.g., measurement with a few wide-bandwidth, high-spatial resolution, bands).

Acknowledgment

Financial support provided by the U.S. NASA Applied Sciences, Ocean Biology and Biogeochemistry (OBB) and Water and Energy Cycle programs, and the Naval Research Laboratory is greatly appreciated. We are extremely grateful to the comments and suggestions from three anonymous reviewers that greatly improved this manuscript.

#172216 - $15.00 USD Received 10 Jul 2012; revised 23 Aug 2012; accepted 24 Aug 2012; published 28 Aug 2012